Solar Energy 188 (2019) 300–304

Contents lists available at ScienceDirect

Solar Energy

journal homepage: www.elsevier.com/locate/solener

Large-area MACE Si nano-inverted-pyramids for PERC solar cell application

Z.G. Huang[a,b,*], K. Gao[a], X.G. Wang[a], C. Xu[a], X.M. Song[a], L.X. Shi[a], Y. Zhang[b], B. Hoex[b], W.Z. Shen[c]

[a] School of Science, School of Chemical Enginering, Huaihai Institute of Technology, Lianyungang 222005, Jiangsu Province, PR China
[b] School of Photovoltaic and Renewable Energy Engineering, UNSW Sydney, Sydney, New South Wales 2052, Australia
[c] Laboratory of Condensed Matter Spectroscopy and Opto-Electronic Physics, and Key Laboratory of Artificial Structures and Quantum Control (Ministry of Education), School of Physics and Astronomy, and Institute of Solar Energy, Shanghai Jiao Tong University, Shanghai 200240, PR China

ARTICLE INFO

Keywords:
Si nanostructures
Solar cells
Nano-inverted-pyramids
High-performance
PERC

ABSTRACT

Silicon (Si) nanostructures are regarded as a competitive candidate for the front texture of future high-efficiency Si solar cells owing to their excellent light-trapping properties. In this paper, we present nano-inverted-pyramids (NIPs) textures on the surface of Cz Si wafer with an area of 156 × 156 mm^2 fabricated by employing the metal-assisted chemical etching (MACE) technique. The optical properties of the surface are investigated in detail before and after the application of a SiO_x/SiN_x antireflection coating. A passivated emitter and rear contact (PERC) solar cell with NIPs (NIPs-PERC) is analyzed at the cell as well module level using simulation. The simulation results indicate that the NIPs-PERC solar cell possesses a higher efficiency (η) of 1.4% relatively than that of the traditional PERC solar cell, benefiting from a significant better reflection performance in both the short as well as long wavelength range. Furthermore, simulations show that a 60-cell module with NIPs-PERC solar cells can yield a peak power of 310 W which is 8 W higher than a traditional PERC module. The novel NIPs-PERC solar cell shows high potential for mass production and opens a broad way for the application of NIPs textures to other high-performance solar cells.

1. Introduction

Due to the near-zero reflection over a broad range of incident angles (Branz et al., 2009; Kafle et al., 2015; Koynov et al., 2006; Liu et al., 2014), silicon (Si) nanostructured textures have attracted considerable interests for application in solar cells, showing an effective way to achieve high efficiencies (ηs) of solar cells. However, the implementation of nanostructured textures in photovoltaic (PV) devices is challenging (Branz et al., 2009; Chen et al., 2011; Es et al., 2015; Fang et al., 2008; Huang et al., 2012; Huang et al., 2015a; Huang et al., 2016; Huang et al., 2015b; Kafle et al., 2015; Kayes et al., 2005; Kumar et al., 2011; Li et al., 2011; Lin et al., 2013; Liu et al., 2014; Nayak et al., 2011; Peng et al., 2010; Shu et al., 2009; Syu et al., 2013; Toor et al., 2011; Wang et al., 2011; Yuan et al., 2009; Zhong et al., 2015a), which is mainly attributed to the high carrier recombination at the surface and in the bulk of Si nanostructures. Nano-inverted-pyramids (NIPs) textures may provide an effective way to improve the efficiency of PV devices due to their superior light-trapping and structural characteristics (Mavrokefalos et al., 2012; Smith and Rohatgi, 1993; Wang et al., 2014). The potential of NIPs is illustrated in the landmark 25.0% efficient solar cell reported by UNSW in the late 1990 s where the inverted pyramids were fabricated using photolithography. Due to its complexity and high-cost, photolithography is not an appealing technique for solar cell manufacturing. On the other hand, metal-assisted chemical etching (MACE) may be a far simpler, lower-cost, and industry-compatible technique to prepare NIPs (Chen et al., 2018; Huang et al., 2015a; Huang et al., 2016; Huang et al., 2015b; Yang et al., 2017; Zhong et al., 2015a). In this paper, we show that highly uniform NIPs texture on the front surface of industry-sized (156 × 156 mm^2) silicon wafers can be obtained by MACE. The measured reflection of NIPs with PECVD-SiO_x/SiN_x antireflection coating shows excellent light-trapping and matches well with simulation. A passivated emitter and rear contact (PERC) solar cell employing NIPs (NIPs-PERC) was analyzed at the cell as well module level using simulation. The simulation results show that the NIPs-PERC solar cell possessed a significant better reflection performance in both the short as well as long wavelength range, resulting in a relative increase η of 1.4%. Furthermore, simulations showed that a 60-cell module with NIPs-PERC solar cells can yield a peak power of 310 W, 8 W higher than than a module with PERC cells with a traditional texture. Hence, based on the experimental and

* Corresponding author at: School of Science, Huaihai Institute of Technology, Lianyungang 222005, Jiangsu Province, PR China and School of Photovoltaic and Renewable Energy Engineering, UNSW Sydney, Sydney, New South Wales 2052, Australia.
E-mail addresses: zghuang@hhit.edu.cn (Z.G. Huang), songxm@hhit.edu.cn (X.M. Song).

https://doi.org/10.1016/j.solener.2019.06.015
Received 12 March 2019; Received in revised form 2 June 2019; Accepted 5 June 2019

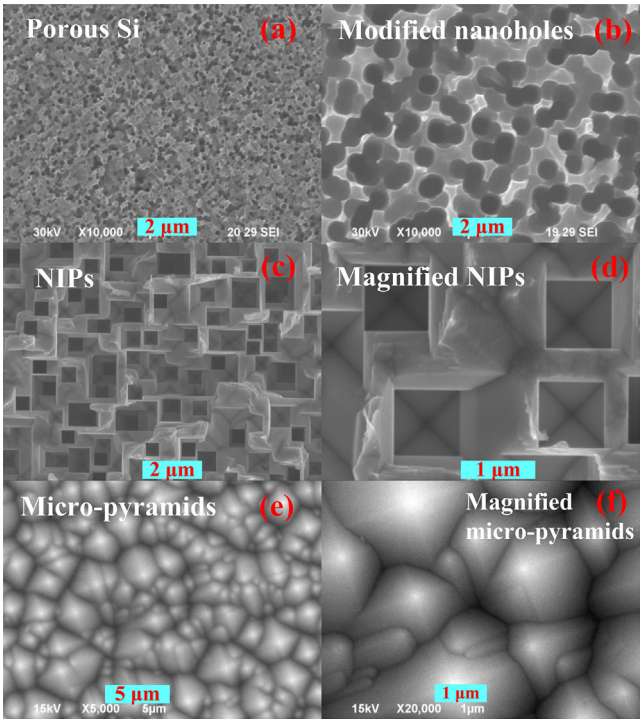

Fig. 1. (a) SEM plan-view image of porous Si obtained by MACE. (b) SEM top view image of the modified nanoholes by following treatment in an HF/HNO_3 solution. (c) SEM plan-view image of NIPs which were obtained by subsequent processing in NaOH solutions. (d) Magnified SEM plan-view image of NIPs. (e) SEM plan-view image of traditional micro-pyramids. (f) Magnified SEM plan-view image of traditional micro-pyramids.

simulation results we believe that MACE-NIPs are an appealing add-on technology for various high-efficiency silicon solar cell architectures such as PERC, all-back contact, and heterojunction solar cells.

2. Experimental

Industry-standard *p*-type (1 0 0) Czochralski-Si (Cz-Si) solar-grade wafers with 156 × 156 mm^2 size, 2-Ωcm-resistivity and 190 ± 10 μm-thickness were used as substrates. After the standard cleaning process, NIPs textures were prepared on the surface of Si wafers as follows: (i) The cleaned Si wafers were immersed in the mixed solutions of $AgNO_3$ (0.0005 M)/HF (4 M)/H_2O_2 (1 M) for 8 min, resulting in porous Si. (ii) Si wafers with porous Si were etched in an HF:HNO_3 = 1:3 (volume) solution at 6 °C for 3 min to smooth the surface morphology and obtain the modified nanoholes. (iii) Nano-inverted-pyramid textures were formed on the surface of Si wafer by the anisotropic etching of 80 °C-NaOH solutions for 2 min. For comparison, traditional pyramid textures were prepared by immersing a Si wafer in a 1.5%-NaOH (mass) solution at 80 °C for 20 min, after the RCA cleaning process of the Si wafer. The deposition of a SiO_x/SiN_x antireflection coating on the front surface of the NIPs and micro-pyramids wafers was performed by PECVD (M82200-6/UM, CETC 48th Research Institute) at a substrate temperature of 400 °C using NO_2/SiH_4 and NH_4/SiH_4 gas mixtures for the SiO_x (~2 nm) and SiN_x (~75 nm) deposition, respectively. Meanwhile, for the measurement of the effective minority carrier lifetimes, the PECVD-SiO_x/SiN_x thin films were symmetrically deposited on both sides of wafers with NIPs and traditional micro-pyramids by the same PECVD process, respectively. Finally, all samples were annealed in atmosphere at 625 °C for 5 min (AF1200-40, Shanghai MicroX).

The morphology of the NIPs was investigated by field emission scanning electron microscopy (SEM) (FE-SEM, FEI Sirion 200). The reflectance spectra were measured on a commercial quantum efficiency measurement system (QEX10, PV Measurements). The effective

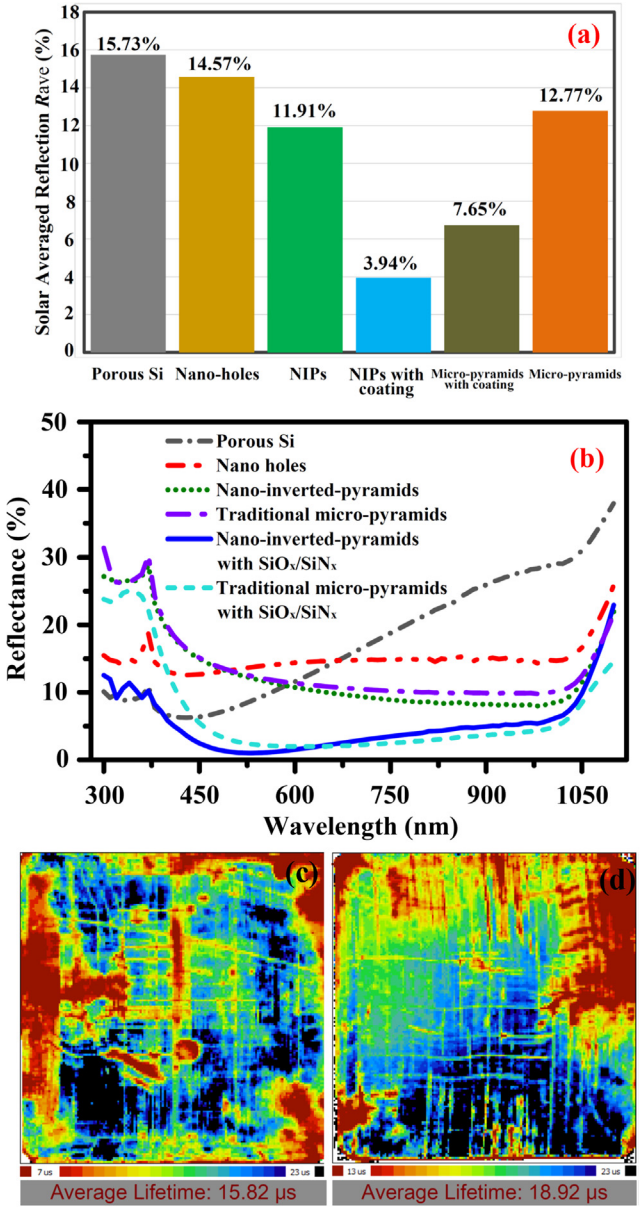

Fig. 2. (a) The solar averaged reflectance R_{ave} and (b) the measured reflectance of four different surface morphology over the 300–1100 nm wavelength range. (c) Effective minority carrier lifetime map of PECVD-SiO_x/SiN_x passivated NIPs (left) and (d) traditional micro-pyramids (right).

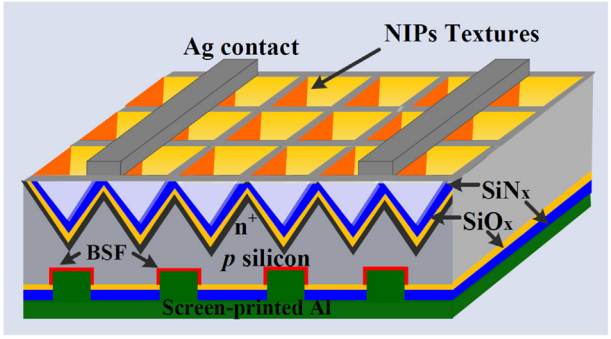

Fig. 3. The schematic device structure of the simulated NIPs-PERC solar cells.

minority carrier lifetimes maps were obtained by microwave photoconductance decay method (WT-2000 SEMILAB). The measured

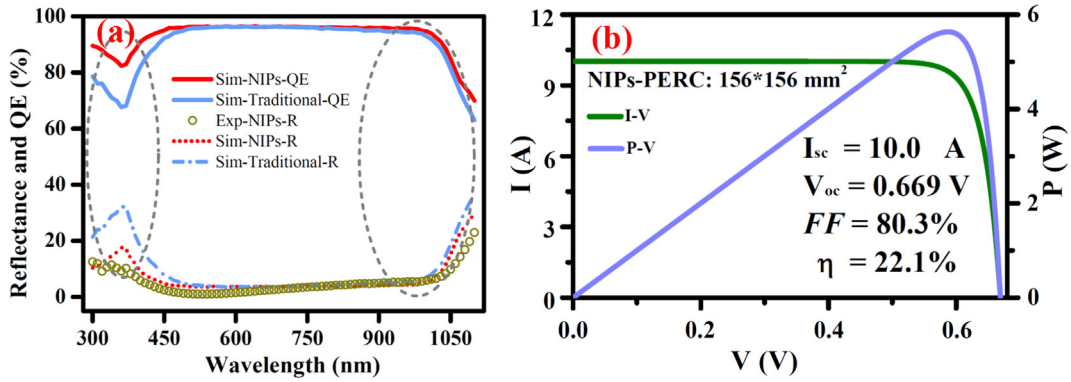

Fig. 4. (a) Simulated reflectance and quantum efficiency (QE) of NIPs-PERC comparing with those of traditional pyramids solar cell. (b) Simulated *I-V* and *P-V* curves of a NIPs-PERC solar cell.

Table 1
Parameters settings of solar cell and module by SunSolve software.

Simulations	Descriptions	Parameters settings
Solar cells	*Wafer*	P-type, Cz, 180 μm-thickness, 2-Ωcm-resistivity, 244 cm^2
	Textures	NIPs-PERC: 1 μm–height Nano-inverted-pyramids Traditional PERC: 3 μm–height Micro-upright-pyramids
	Antireflection coatings	SiO_x (2 nm)/SiN_x (78 nm)
	Rear surface passivation	SiO_x (5 nm)/SiN_x (250 nm)/AlSi (2 μm)
	Solar cell model	Duodiode
	Saturation current J_{01}	237 fA/cm^2
	Ideality factor m_1	1
	Saturation current J_{02}	271nA/cm^2
	Ideality factor m_2	2
	Shunt resistance R_{sh}	18.3 kΩ·cm^2
	Series resistance R_s	0.58 Ω·cm^2
	Busbars	5 BB, height: 35 μm, width: 500 μm
	Fingers	90 fingers, height: 35 μm, width: 45 μm
Modules	*Cell numbers*	60
	EVA thickness	0.45 mm
	Glass thickness	2 mm

Table 2
Simulated output performance NIPs solar cell and module comparing with those of traditional one.

Simulations	Textures	P_{max}(W)	V_{oc}(V)	I_{sc}(A)	*FF*(%)	E_{ff}(%)
Solar cells	Traditional PERC	5.33	669	9.93	80.3	21.8
	NIPs-PERC	5.38	669	10.0	80.3	22.1
Modules(60 cells)	Traditional PERC	302	667	9.36	80.5	20.6
	NIPs-PERC	310	668	9.61	80.4	21.2

reflectance was fitted, and subsequently, the output performance of the solar cells and modules was simulated using the commercial ray-tracing software SunSolve (SunSolve™, 2019).

3. Morphology and optical properties

Fig. 1(a)–(d) shows the progression of the silicon surface from porous silicon to NIPs by plan-view SEM images. Fig. 1(a) shows the porous Si morphology of Si wafer after etching in $AgNO_3/HF/H_2O_2$. Nanoscale porous Si was uniformly distributed on the surface of Si wafer, and the porous silicon feature size could be estimated at 50–100 nm. To obtain larger nanoholes, we modify the Si porous surface by isotropic etching in HF/HNO_3. As shown in Fig. 1(b), nanoholes with an average diameter being ~800 nm formed on the surface of Si wafer and the irregular clusters which are visible in Fig. 1(a) were removed which is beneficial to the formation of the sub-micrometre NIPs. Subsequently, NIPs shown in Fig. 1 (c) were obtained by anisotropic etching in an 80 °C-NaOH solution. The SEM plan-view images show that the surface is quite uniformly covered with NIPs, which is beneficial to the output performance of the solar cell. Fig. 1(d) shows the magnified SEM plan-view image of NIPs and the opening side length and depth of NIPs were estimated as ~840 nm and ~ 600 nm, respectively. For comparison, we prepared the micro-pyramids on the surface of the same Cz-Si wafer by a standard industrial process on a production line. As expected, the prepared mono texture was a micro-pyramid structure with a height of ~3 μm and a width of ~4 μm as shown in Fig. 1(e) and (f), possessing a larger feature size than NIPs. The most important difference between a traditional pyramid texture and NIPS is that light undergoes one or two additional bounces than that in traditional micro-pyramids before being lost by reflection (Wang et al., 2014), attributing to a better light-trapping effect in the short- wavelength range.

To investigate the optical properties of the NIPs textures, we calculate the solar averaged reflectance R_{ave} over the wavelength range 300–1100 nm (see Fig. 2(a)), and compare the reflectance of the NIPs texture with the other morphologies corresponding to different intermediate processes as shown in Fig. 2(b). We calculate the solar averaged reflectance R_{ave} by averaging the reflectance over the AM1.5 spectrum in the wavelength range 300–1100 nm as follows:

$$R_{ave} = \frac{\int_{300\,nm}^{1100\,nm} R(\lambda)\cdot S(\lambda)\cdot d\lambda}{\int_{300\,nm}^{1100\,nm} S(\lambda)\cdot d\lambda} \quad (1)$$

where $R(\lambda)$ and $S(\lambda)$ denote the measured reflectance and AM1.5 solar photon spectral distribution, respectively. As shown in Fig. 1(a), the R_{ave}s of porous Si, nano-holes, NIPs, NIPs with SiO_x/SiN_x coating are 15.73%, 14.57, 11.91% and 3.94%, respectively, meaning a decreasing trend of R_{ave}s with the etching processes. Importantly, compared to the corresponding R_{ave} of traditional micro-pyramids without (12.77%) and with SiO_x/SiN_x coating (7.65%), both NIPs and NIPs with SiO_x/SiN_x coating have an obvious reflection superiority which is beneficial to the short-circuit current of the device.

For the reflectance over the whole wavelength range of 300–1100 nm, the porous Si has a low reflection in the short wavelength range of 300–450 nm and a noticeable increase in reflection from 550 to 850 nm as shown in Fig. 2 (b). As expected, porous Si with a feature size of 60–100 nm can trap short wavelength light, while it is increasingly seen an “effective medium” consisting of silicon and air for larger wavelengths (Branz et al., 2009). After the HF/HNO_3 etch, the nanohole-covered surface shows a higher reflection in the 300–450 nm wavelength range due to the smoothing of the surface, while the reflectance in the 550–1000 nm range is significantly reduced due to a combination of a smooth surface and light trapping by the nano-holes. The sample with the NIPs shows a higher reflectance in the short

wavelength range of 300–450 nm which can be attributed to the fact that the feature size of the NIPs is significantly larger than the wavelength and, consequently, the reflection is determined by normal geometrical optics. However, compared to the traditional micro-pyramids, the uncoated NIPs possess better light trapping properties over the whole wavelength range which can be attributed to triple or more bounces in the NIP structures before the light escapes from the surface (Mavrokefalos et al., 2012). Importantly, for the PECVD-SiO_x/SiN_x capped case, both the NIPs and micro-pyramids show a sharp reduction of the reflectance over the whole 300–1100 nm wavelength range, and the reflectance difference between the PECVD-SiO_x/SiN_x coated NIP and traditional pyramids is even further magnified in the wavelength range of 300–600 nm. The major reasons for such a magnified reflectance difference after PECVD-SiO_x/SiN_x deposition may lie in the wafer-scale non-uniformity, the better geometric optics antireflection and the enhanced destructive interference of the PECVD-SiO_x/SiN_x coated NIPs arrays (Zhong et al., 2015b).

Now, we turn to the measured lifetimes of the effective minority charge carriers for PECVD-SiO_x/SiN_x passivated NIPs and traditional micro-pyramids, which is an important parameter to reflect the electrical properties of the samples. As shown in Fig. 2, the average lifetime of PECVD-SiO_x/SiN_x coated NIPs was 15.82 μs, indicating an identical passivation level as the passivated micro-pyramids with a lifetime value of 18.92 μs. This is not surprising as the effective surface area of the two textures is expected to be equal at roughly 1.74 times that of a planar sample. Furthermore, the pit structure of NIPs might be beneficial for subsequent contacting (Wang et al., 2014). In a word, the excellent light-trapping and electrical properties make NIPs an attractive texturing for the Si high-performance photovoltaic devices such as PERC, all-back contact, and heterojunction solar cells.

4. Simulated performance of NIPs-PERC solar cells and modules

Fig. 3 shows the schematic device structure of the NIPs-PERC. It consists of a MACE-NIPs texture with a SiO_x/SiN_x stack on an n^+ emitter. The rear reflector consisted of a SiO_x/SiN_x stack with a screen-printed Al with locally alloyed rear contacts.

Using the SunSolve software, we simulated the reflectance and quantum efficiency (QE) of NIPs-PERC solar cell as shown in Fig. 4(a). The detailed simulation parameters settings are listed in Table 1. Note that we set the feature size of the optimized NIPs as 1-μm which is fully in the geometric optics regime and is suitable for the simulation based on ray-tracing SunSolve software (Payne et al., 2018). As shown in Fig. 4(a), the measured reflectance of NIPs with PECVD-SiO_x/SiN_x is much lower than that of the simulated one in the wavelength range of 300–700 nm. Hence, the simulated values will underestimate the true potential of the NIPs. Notably, in both the 300–500 nm wavelength range and the 900–1050 nm wavelength range, the simulated reflectance of NIPs capped by SiO_x/SiN_x is lower than that of traditional micro-pyramids resulting in a significantly improved simulated QE of a NIPs-PERC solar cell.

Benefiting from a superior optical performance of the NIPs compared to the random pyramids, the NIPs-PERC solar cell demonstrates a very high performance with a high short-circuit current of 10.0 A, an open-circuit voltage (V_{oc}) of 0.669 V, a fill factor (*FF*) of 80.3%, as well as power conversion efficiency (η) of 22.1% as shown in Fig. 4 (b) (see parameters settings in Table 1). Compared to the PERC solar with random pyramids, the NIPs-PERC solar cell has a simulated increase of 70 mA while the V_{oc} and *FF* are not affected, consequently increasing the η from 21.8% to 22.1% (a relative increase of 1.4%). Furthermore, we simulate the performance of a standard NIPs-PERC module with 60 cells (see Table 2). The module power of NIPs-PERC was simulated to be 311 W, which is 1.3% relatively higher than the 307 W simulated for the module with random pyramid solar cells.

5. Conclusions

By optimising the morphology of MACE porous Si and acid modified nanoholes, we prepared highly uniform NIPs texture on the front surface of industry-sized ($156 \times 156\ mm^2$) silicon wafers under the anisotropic etching of NaOH. The measured reflection curve shows that the NIPs capped by PECVD-SiO_x/SiN_x demonstrates a lower reflection than traditional micro-pyramids. Subsequently, we analyzed passivated emitter and rear contact (PERC) with NIPs (NIPs-PERC) at cell as well module level using simulation. The simulation results show the NIPs-PERC solar cell can reach a η of 22.1% which is 1.4% relative higher than that of the traditional PERC as a result of the better reflection performance in both the short as well as long wavelength range. Furthermore, the simulation of a 60-cell PV module with NIPs-PERC solar cells yields a peak power of 310 W module which is 8 W higher compared to a traditional PERC module. These experimental and simulation results demonstrate that MACE-NIPs possess a great potential to be used in various high-efficiency Si solar cell architectures.

Acknowledgements

This work was supported by the Natural Science Foundation of China (61774069 and 11834011), the Natural Science Foundation of Jiangsu Province (BK20151284), the “333” Project of Jiangsu Province, the “Qinglan” Project of Jiangsu Education Department” and the Open Project of Key Laboratory of Artificial Structures and Quantum Control (Ministry of Education).

References

Branz, H.M., Yost, V.E., Ward, S., Jones, K.M., To, B., Stradins, P., 2009. Nanostructured black silicon and the optical reflectance of graded-density surfaces. Appl. Phys. Lett. 94 (23), 1850.
Chen, C., Rui, J., Li, H., Meng, Y., Liu, X., Ye, T., Kasai, S., Tamotsu, H., Wu, N., Wang, S., 2011. Electrode-contact enhancement in silicon nanowire-array-textured solar cells. Appl. Phys. Lett. 98 (14), 885.
Chen, K., Zha, J., Hu, F., Ye, X., Zou, S., Vähänissi, V., Pearce, J.M., Savin, H., Su, X., 2018. MACE nano-texture process applicable for both single- and multi-crystalline diamond-wire sawn Si solar cells. Sol. Energy Mater. Sol Cells, pp. 191.
Es, F., Ciftpinar, E.H., Demircioglu, O., Gunoven, M., Kulakci, M., Turan, R., 2015. Performance of solar cells fabricated on black multicrystalline Si by nanowire decoration. Appl. Surf. Sci. 332, 266–271.
Fang, H., Li, X., Song, S., Xu, Y., Zhu, J., 2008. Fabrication of slantingly-aligned silicon nanowire arrays for solar cell applications. Nanotechnology 19 (25), 255703.
Huang, B.R., Yang, Y.K., Lin, T.C., Yang, W.L., 2012. A simple and low-cost technique for silicon nanowire arrays based solar cells. Sol. Energy Mater. Sol. Cells 98 (98), 357–362.
Huang, Z., Lin, X., Zeng, Y., Zhong, S., Song, X., Liu, C., Yuan, X., Shen, W., 2015a. One-step-MACE nano/microstructures for high-efficient large-size multicrystalline Si solar cells. Sol. Energy Mater. Sol. Cells 143, 302–310.
Huang, Z., Song, X., Zhong, S., Xu, H., Luo, W., Zhu, X., Shen, W., 2016. 20.0% Efficiency Si nano/microstructures based solar cells with excellent broadband spectral response. Adv. Funct. Mater. 26 (12), 1892–1898 20.0%.
Huang, Z., Zhong, S., Hua, X., Lin, X., Kong, X., Dai, N., Shen, W., 2015b. An effective way to simultaneous realization of excellent optical and electrical performance in large-scale Si nano/microstructures. Progress Photovolt. Res. Appl. 23, 964–972.
Kafle, B., Mannan, A., Freund, T., Clochard, L., Duffy, E., Hofmann, M., Rentsch, J., Preu, R., 2015. Nanotextured multicrystalline Al-BSF solar cells reaching 18% conversion efficiency using industrially viable solar cell processes. physica status solidi. (RRL) - Rapid Res. Lett. 9 (8), 448–452.
Kayes, B.M., Atwater, H.A., Lewis, N.S., 2005. Comparison of the device physics principles of planar and radial p-n junction nanorod solar cells. J. Appl. Phys. 97 (11), 610–1149.
Koynov, S., Brandt, M.S., Stuttzmann, M., 2006. Black nonreflecting silicon surfaces for solar cells. Appl. Phys. Lett. 88 (20), 203107.
Kumar, D., Srivastava, S.K., Singh, P.K., Husain, M., Kumar, V., 2011. Fabrication of silicon nanowire arrays based solar cell with improved performance. Sol. Energy Mater. Sol. Cells 95 (1), 215–218.
Li, Y., Yu, H., Li, J., Wong, S.-M., Sun, X., Li, X., Cheng, C., Fan, H., Wang, J., Singh, N., 2011. Novel silicon nanohemisphere-array solar cells with enhanced performance. Small 7 (22), 3138–3143.
Lin, X., Hua, X., Huang, Z., Shen, W., 2013. Realization of high performance silicon nanowire based solar cells with large size. Nanotechnology 24 (23), 235402.
Liu, X., Coxon, P.R., Peters, M., Hoex, B., Cole, J.M., Fray, D.J., 2014. Black silicon: fabrication methods, properties and solar energy applications. Energy Environ. Sci. 7, 3223–3263.

Mavrokefalos, A., Han, S.E., Yerci, S., Branham, M.S., Chen, G., 2012. Efficient light trapping in inverted nanopyramid thin crystalline silicon membranes for solar cell applications. Nano Lett. 12 (6), 2792.
Nayak, B.K., Iyengar, V.V., Gupta, M.C., 2011. Efficient light trapping in silicon solar cells by ultrafast-laser-induced self-assembled micro/nano structures. Progress Photovolt. Res. Appl. 19 (6), 631–639.
Payne, D., Fung, T., Khan, M.U.K., Cruz-Campa, J., McIntosh, K., Abbott, M., 2018. Understanding the optics of industrial black silicon. AIP Conf. Proc. 1999, 050007.
Peng, K., Yu, Y., Wu, Y., Yan, Y., Lee, S.-T., Zhu, J., 2010. Aligned single-crystalline Si nanowire arrays for photovoltaic applications. Small 1 (11), 1062–1067.
Shu, Q., Wei, J., Wang, K., Zhu, H., Li, Z., Jia, Y., Gui, X., Guo, N., Li, X., Ma, C., 2009. Hybrid heterojunction and photoelectrochemistry solar cell based on silicon nanowires and double-walled carbon nanotubes. Nano Lett. 9 (12), 4338–4342.
Smith, A.W., Rohatgi, A., 1993. Ray tracing analysis of the inverted pyramid texturing geometry for high efficiency silicon solar cells. Sol. Energy Mater. Sol. Cells 29 (1), 37–49.
SunSolve™, P.L., 2019. < https://www.pvlighthouse.com.au > .
Syu, H.J., Shiu, S.C., Hung, Y.J., Hsueh, C.C., Lin, T.C., Subramani, T., Lee, S.L., Lin, C.F., 2013. Influences of silicon nanowire morphology on its electro-optical properties and applications for hybrid solar cells. Progress Photovolt. Res. Appl. 21 (6).
Toor, F., Branz, H.M., Page, M.R., Jones, K.M., Yuan, H.C., 2011. Multi-scale surface texture to improve blue response of nanoporous black silicon solar cells. Appl. Phys. Lett. 99.
Wang, X., Peng, K., Pan, X., Chen, X., Yang, Y., Li, L., Meng, X., Zhang, W., Lee, S.-T., 2011. High-performance silicon nanowire array photoelectrochemical solar cells through surface passivation and modification. Angew. Chem. Int. Ed. Engl. 50 (42), 9861–9865.
Wang, Y., Yang, L., Liu, Y., Mei, Z., Chen, W., Li, J., Liang, H., Kuznetsov, A., Du, X., 2014. Maskless inverted pyramid texturization of silicon. Sci. Rep. 5, 10843.
Yang, L., Liu, Y., Yan, W., Wei, C., Chen, Q., Wu, J., Kuznetsov, A., Du, X., 2017. 18.87%-efficient inverted pyramid structured silicon solar cell by one-step Cu-assisted texturization technique. Sol. Energy Mater. Sol. Cells 166, 121–126.
Yuan, H.C., Yost, V.E., Page, M.R., Stradins, P., Meier, D.L., Branz, H.M., 2009. Efficient black silicon solar cell with a density-graded nanoporous surface: optical properties, performance limitations, and design rules. Appl. Phys. Lett. 95 (12), 19–1586.
Zhong, S., Huang, Z., Lin, X., Zeng, Y., Ma, Y., Shen, W., 2015a. High-efficiency nanostructured silicon solar cells on a large scale realized through the suppression of recombination channels. Adv. Mater. 27 (3), 555–561.
Zhong, S., Zeng, Y., Huang, Z., Shen, W., 2015b. Superior broadband antireflection from buried Mie resonator arrays for high-efficiency photovoltaics. Sci. Rep. 5, 8915.